Ocean Sci. Discuss., 9, 2327–2373, 2012
www.ocean-sci-discuss.net/9/2327/2012/
doi:10.5194/osd-9-2327-2012

Ocean Science Discussions

Arctic rapid sea ice loss events in regional coupled climate scenario experiments

R. Döscher and T. Koenigk

SMHI/Rossby Centre Folkborgsvägen 1, 60176 Norrköping, Sweden

Received: 29 May 2012 – Accepted: 4 June 2012 – Published: 9 July 2012

Correspondence to: R. Döscher (ralf.doescher@smhi.se)

Published by Copernicus Publications on behalf of the European Geosciences Union.

Abstract

Rapid sea ice loss events (RILEs) in a mini-ensemble of regional Arctic coupled climate model scenario experiments are analyzed. Mechanisms of sudden ice loss are strongly related to atmospheric circulation conditions and preconditioning by sea ice thinning during the seasons and years before the event. Clustering of events in time suggests a strong control by large scale atmospheric circulation. Anomalous atmospheric circulation is forcing ice flow and providing warm air affecting winter ice growth. Even without a seasonal preconditioning during winter, ice drop events can be initiated by anomalous inflow of warm air from the Atlantic sector during summer. It is shown that RILE events can be generated solely based on atmospheric circulation changes without possible competing mechanisms, such as anomalous seasonal radiative forcing or short-lived forcers (e.g. soot). Such forces do merely play minor roles or no role at all in our model. Mechanisms found are qualitatively in line with observations of the 2007 RILE.

1 Introduction

The observed development of Arctic sea ice extent since the start of satellite observations in 1979 shows a long term trend towards less ice, superimposed by interannual variability. For the annual summer minimum during September, new recent record minimum values have been observed during 2002, 2005 and 2007. By 2007, the average September extent trend since 1979 was 0.072×10^6 km^2 per year (Stroeve et al., 2008). The 2007 event marked an unprecedented ice extent loss in the observed history downwards from 5.55×10^6 km^2 in September 2005 to 4.28×10^6 km^2 in September 2007.

Existing analysis of the observed 2007 event covers preconditioning, dynamic and radiative atmospheric forcing and mechanisms leading to increased bottom melting. There is broad agreement on a multi-year trend of ice thinning and a low perennial ice coverage in previous years, which sets the stage for unusual, but not unprecedented

OSD
9, 2327–2373, 2012

atmospheric conditions to generate the 2007 event. The March 2007 sea ice extent and area were among the lowest three ever observed since the start of satellite observations in 1979 (Comiso et al., 2008).

During spring and early summer 2007, two surface pressure anomalies were established over the wider Arctic area. A sea level pressure (SLP) below normal over Siberia and the Laptev Sea was coinciding with positive conditions of the Northern Annular Mode (NAM) (Maslanik et al., 2007). Over the central Arctic and northern Canada, a high pressure anomaly occurred and persisted for three months. It was dominated by a strongly positive phase of the Pacific-North American (PNA) pattern (L'Heureux et al., 2008), a large-scale wave pattern featuring a sequence of high- and low-pressure anomalies stretching from the subtropical west Pacific to North America with a high pressure anomaly in the very north.

That specific combination of cyclonic and anticyclonic anomalies over the Arctic constitutes a dipole structure with meridional winds giving rise to advection of sea ice from the Pacific to the Atlantic sector of the Arctic accounting for about 15 % of the total ice retreat in the Pacific sector (Kwock, 2008). Another effect was above-average air temperatures north of Siberia. The dipole pressure pattern had become more frequent in the winters and springs of the years before 2007, but persistence of this pattern through summer is unusual (Maslanik et al., 2007) and reasons for that persistence are unclear.

Associated with the anticyclonic (high pressure) anomaly over the western part of the Arctic, reduced cloudiness and enhanced downwelling radiation were found, which could have contributed to melting in the Pacific sector of the Arctic ocean. Increased melting from the bottom of the sea ice in the Beaufort Sea was found by means of ice mass balance observations (Perovich et al., 2008). The primary source of heat was provided by solar radiation through increased fractions of open water. Additional solar heating due to a period of reduced cloud cover could have played a role. (Francis and Hunter, 2006; Kay et al., 2008). That hypothesis was questioned by experiments with a coupled ocean-sea ice model (Schweiger et al., 2008) forced by a negative cloud anomaly and increased shortwave flux from June through August. No substantial contribution to the record sea ice extent minimum was found.

The overall picture of the 2007 event is diverse and different possible specific mechanisms have been suggested, involving preconditioning, large scale atmospheric variability, and local processes. Taking an integrated view based on a coupled ocean-sea ice simulation and using adjoint methods, Kauker et al. (2009) found that the 2007 summer sea ice event can be traced back to four major influences: the March sea ice thickness, May and June wind conditions favoring ice transport towards Fram Straits, and September surface air temperature.

Similar to the situation after earlier record minimum events, a partial recovery of the sea ice extent is observed after 2007. Based on the previously observed record, it appears likely that new events could follow the 2007 event. Therefore it is relevant to ask for the possible frequency of rapid change events and the range of possible underlying mechanisms and forcing situations. When it comes to probability and character of possible future RILE's, we need to consult numerical projections of future climates in the Arctic, responding to increasing atmospheric greenhouse gas concentrations. Global climate models (GCMs) provide such scenario projections. By 2007, RILEs were rarely simulated in global climate simulations. Sea ice extent projections from several GCMs were compiled by the CMIP3 project (Zhang and Walsh, 2006). The amplitude of the observed 2007 event was far outside the variability of the GCM ensemble. Dissenting results in the CCSM GCM was given e.g. by Holland et al. (2006), showing ice loss events.

Regional dynamical downscaling of GCM scenario projections ("regional scenario") provides regional interpretation of global change with increased resolution. In this paper we present an analysis of several rapid sea ice loss events (RILE's), based on scenario downscaling experiments with a regional coupled climate model of the Arctic. Our Arctic regional scenario experiments show a realistic level of sea ice extent in the Arctic ocean for recent climate (Koenigk et al., 2011). All our regional scenarios show rapid change events in summer sea ice extent. Those events consist of distinct drops in sea ice extent during one or more years in a row. After the event, a partial recovery is typically seen. Our analysis of RILE's aims at identifying relevant mechanisms for the drop and recovery of sea ice extent.

Starting with descriptions of the regional model and the experimental setup, we describe spatially averaged time series of sea ice related fields and an average RILE event. The role of the Arctic Dipole anomaly pattern for the most extreme events is explored. Composites of the several events are presented to document the role of different mechanisms, and eventually three single events of varying character are analyzed. Conclusions are drawn regarding major mechanisms of preconditioning and ice loss.

2 Model data and experiments

To analyze rapid sea ice change events we use six Arctic regional climate scenario experiments performed with the Rossby Centre Atmosphere Ocean model RCAO (Döscher et al., 2002, 2009). All runs are performed as regional dynamic downscaling of global scenarios projections by the Max Planck Institute climate model ECHAM5/MPI-OM (here: "the GCM") applying the A1B emission scenario as used for the CMIP3 project.

RCAO consists of the atmosphere component RCA and the ocean component RCO. The model area extends from about 50° N in the Atlantic sector across the Arctic to the Aleutian Island chain in the North Pacific as illustrated e.g. in Fig. 3a. Both RCO and RCA run in a horizontal resolution of 0.5° on a rotated latitude-longitude grid with the grid equator crossing the geographical North Pole. The ocean component RCO has been described and verified for the Arctic (Döscher et al., 2009) and for a Baltic Sea domain (Meier et al., 2003). RCO comprises a dynamic-thermodynamic sea ice model based on an elastic-viscous-plastic (EVP) rheology (Hunke and Dukowicz, 1997) and a Semtner-type thermodynamics (Semtner, 1976). The ice and snow albedo formulation is based on a modified version of Koltzow (2007) with albedo values dependent on the

OSD
9, 2327–2373, 2012
Arctic rapid sea ice loss events
R. Döscher and T. Koenigk

ice surface temperature. A parameterization for melt ponds is included. RCO has 59 unevenly spaced vertical levels. A closed lateral boundary exists at the Aleutian Island chain and open lateral boundary conditions in the North Atlantic Ocean. In the case of inflowing water, climatologically monthly mean temperature and salinity data from the PHC data set (Steele et al., 2001) or monthly ocean data from global scenario simulations of the Max Planck Institute climate model ECHAM5/MPIOM are used. Depeding on the run, sea surface salinity is restored to the PHC climatology on a timescale of 240 days, or it is modified by a salinity flux correction (see Koenigk et al., 2011). This treatment is necessary to prevent artificial salinity drift due to insufficient provision of freshwater runoff and precipitation.

The atmosphere component RCA has been described by Jones et al. (2004a, b) and Kjellström et al. (2005). The current model set up has 24 vertical layers in terrain-following hybrid coordinates with a model top at approximately 15 hPa. As lateral boundary forcing, atmospheric data from ECHAM5/MPI-OM is taken and updated with a 6-hourly frequency. Later improvements of RCA are described in Kjellström et al. (2005), Samuelsson et al. (2006) and Döscher et al. (2009). Both models RCO and RCA exchange information via a separate coupler software OASIS4 (Valcke and Redler, 2006) with a coupling frequency of three hours.

The regional RCAO scenario experiments are started 1 April 1960 and end 31 December 2080. All regional runs were initialized with GCM atmospheric fields and ocean temperature and salinity from the PHC climatology (Steele et al., 2001). Sea ice was initialized with a constant thickness of 2.3 m and a concentration of 95 % for ocean gridboxes with a sea surface temperature (SST) colder or equal to the freezing temperature. After 20 yr of simulation between 1960 and 1979, the ocean fields are considered in advective balance. As shown in Döscher et al. (2009), trend and mean values of sea ice extent after 20 yr of integration is similar to observations during the 1980s and 1990s, when RCAO is forced with ERA-40 reanalysis at the lateral boundaries.

Our regional experiments use A1B scenario simulations of the last IPCC Assessment Report from ECHAM5/MPI-OM as forcing at the lateral boundaries. Radiative effects

OSD
9, 2327–2373, 2012

R. Döscher and T. Koenigk

of the A1B greenhouse gas concentrations are prescribed even within the atmospheric component of RCAO.

Our six experiments were initially designed as a sensitivity study and climate change projection experiment. The set-up varies in forcing and sea ice parameters. Four out of our six experiments have been used for the climate change study of Koenigk et al. (2011). In some experiments, only the atmospheric fields of the global climate model (GCM) are used at the lateral boundaries, while the ocean boundaries are prescribed using climatological values. In addition, simulations have been performed with lateral forcing from both ocean and atmosphere of ECHAM5/MPI-OM. Certain runs utilize sea surface salinity restoring while others use salinity flux correction (see Koenigk et al., 2011). Different values for the freezing height of lateral freezing (see Döscher et al., 2009) are used to generate thinner or thicker sea ice conditions. All regional runs are forced by identical lateral atmosphere forcing from ECHAM5/MPI-OM. Al runs utilize identical setups for the atmosphere component RCA.

3 Definition of a rapid sea ice change event

A rapid sea ice loss event (RILE) in this study is a temporary reduction of the annual minimum of sea ice extent during summer. In the Arctic, the minimum occurs during September. Here we define a RILE as a drop of summer sea ice extent by more than 1 200 000 km^2 overall. The event can consist of one big drop ("one-step event") or of up to three consecutive steps of smaller year-to-year drops in a row ("multi-year event"). The first step is considered part of the event if it is larger than 500 000 km^2. Later on, the events are compared with average conditions of the respective 10-yr period directly before the start of the event. We are excluding events with strong variability during the 10-yr-reference period. In the 6 regional scenario runs, we pick the first respective 5 events, which leaves us with a total of 30 events for analysis: 9 one-step events and 21 multi-year events.

4 Results

4.1 Long term trends and clustering of rapid ice loss events

Spatial averages of seasonal means (JFM for winter and JAS for summer) for key variables have been calculated north of 70° N over the sea ice covered area with at least 15 % of ice coverage (Fig. 1). In all ensemble runs overall trends are clearly visible. Over the 100-yr period 1980–2079, summer sea ice extent is decreasing (Fig. 1a), as is thickness (Fig. 1b) during summer and winter.

The increase of 2 m air temperature (T2M, Fig. 1d) is strongest during winter (8–10 K). Winter sea surface temperature (SST, Fig. 1c) change is much more limited (about 0.5 K) due to the isolating ice cover and almost constant freezing point temperatures directly underneath the ice. Summer T2M and SST are increasing both with roughly 2–3 K (note different ordinate scaling in Fig. 1) due to enlarged areas of leads and open water.

The strongest signal in melting and freezing rates is seen in the increasing summer melting at the ice bottom (Fig. 1e), which must be connected to water warming underneath the ice. A weaker increase is seen in the spring surface melting (no figure), while summer surface melting is decreasing. This is consistent with summer ice margins closer to the pole on average.

From the sea ice extent curve (Fig. 1a), it becomes clear that rapid loss events are followed by at least partial recoveries. This behavior is typical even for the observed summer extent time series (e.g. Stroeve et al., 2008). It opens for the possibility of negative feedbacks in response to the event. Alternatively, it might indicate that conditions suitable for generating a loss event exist only for a limited number of years before less favorable conditions reoccur independently of the ice loss.

Variability on top of the trends show some intra-ensemble coherence on decadal scale and in some cases even on the annual scale. This is clearly visible for e.g. sea ice extent, SST and T2M. While the long term variability of extent is beyond our scope, we are interested in the sea ice loss events and its intra-ensemble coherence. Before 2025, ensemble members show largely individual behavior with respect to occurrence of a rapid loss events, although clustering of 2–3 ensemble members occurs. After 2025, events are mostly clustered within at least 4 ensemble members in periods of 3–5 yr. This coherence suggests some degree of controlling by large scale conditions given by identical atmospheric conditions prescribed at the lateral boundaries of the regional model domain. Still, even after 2025, a minority of cases does not participate in the clustering of events. Thus conditions and processes specific to the individual ensemble runs are essential and can overrule a dominating large scale influence emanating from identical lateral boundary conditions.

As an example of clustering, we take a closer look at the events during the period 2030–2035 to learn about preferred conditions for clustering. During that period, 5 out of 6 members show an event, and the sixth member is close to an event. We compare the SLP of the event with a reference period of 10 yr before the event (Fig. 2). We consider the average winter before an event and the average event summer itself. Both show a distinct high surface pressure anomaly over Alaska and northern Canada. During winter, the high anomaly is complemented by a pronounced negative anomaly covering most of the Arctic ocean and centered over the Laptev sea reaching into northern Europe and Siberia. This indicates a broad inflow of air from the Pacific ocean into large parts of the central Arctic ocean and towards the Canada and Greenland coast, connected to sea ice drift from the Chukchi and eastern Siberian Seas towards Canada and Greenland. During summer, the SLP anomaly is dominated by high pressure over the Beaufort Sea including the North American coast, and another high pressure anomaly over the wider Greenland area, which also gives rise to atmospheric inflow from the Pacific across the Arctic ocean. The summer sea ice thickness anomaly (Fig. 2c) shows strongest thinning in the Chukchi Sea, eastern Siberian Sea and Laptev Sea. Those are the conditions of sea ice loss events during a certain time period of strong large scale control. The anomalies shown explain the forcing mechanism of the events, but not why all ensemble members generate an event at about the same time. Compared with the overall 30-event average (Fig. 3) we find that the sea

OSD
9, 2327–2373, 2012

ice reduction during the clustering phase is very much concentrated on the Siberian coastal Seas, while the 30-yr average shows reduction in almost all of the Arctic ocean. We conclude that atmospheric conditions supporting ice loss in the Siberian coastal Seas, provide a strong constraint to generate a RILE. Most of our 30 events show some ice left at the east-Siberian coast. This is a feature of many Arctic or global climate models (e.g. Gerdes and Köberle, 2007; Blanchard et al., 2011). If this can be counteracted by specific large scale atmospheric conditions, we have a strong potential for common RILEs within the ensemble, largely independent of local conditions or possible feedbacks.

Taking into account that thick ice off Siberia might be an unrealistic feature, given existing high pressure biases (Cassano et al., 2011) and the effects of not considering multiple ice classes (Vancoppenolle, 2008), the described dominance of large scale atmospheric conditions, as expressed by clustering in the model experiments, might be less important in reality.

4.2 The average rapid sea ice loss event

Sea ice rapid change events differ in the importance of specific mechanisms and the location of ice reduction. Analyzing an average event gives insights into dominating features valid for most events. More detailed understanding of processes needs to be derived from specific analysis such as composites (Sect. 4.4) and specific case studies (Sect. 4.5).

Here we present average seasonal anomaly fields over all 30 events including the year of the event. If an event consists of more than one step (i.e. several consecutive drops of summer extent in a row), all steps are taken into account and averaged into one average seasonal cycle of the event year. Each single anomaly field represents the difference between the respective season and the corresponding 10 yr seasonal mean before the start of the event. The average over all 30 events gives us anomalies for the seasons characterizing both an average RILE and an average recovery year after the

OSD
9, 2327–2373, 2012

event. Resulting fields are shown in Fig. 3a for the event and in Fig. 3b for the recovery. Melting rates for bottom and top of the ice are given in Fig. 3c.

The average winter (JFM, Fig. 3a, upper row) before the average summer event shows a distinct T2M rise over all the Arctic ocean and adjacent land areas, with a maximum warming of up to 2 K over the Chukchi Sea. That warming appears to be consistent with a winter SLP anomaly associated with warm air transport from the Pacific area into the Arctic. This corresponds to a weakening of the typical wintertime zonal transport in the Arctic. Other winter anomalies are rather small: sea ice concentration (SIC) reduction is limited to the winter ice margin. Winter sea ice thickness is reduced by up to 35 cm away from the northern Greenland and Canada coastal area. SST anomalies (no figure) reflect SIC changes. The SLP anomaly shows similarities with Fig. 2 which represents the conditions of efficient large scale forcing of a RILE in the coming summer. A small but decisive difference is the weaker depression centered over the Kara Sea implying no direct ice drift from the East-Siberian shelf towards Canada and Greenland.

During spring (AMJ, Fig. 3a, second row) before the summer event, T2M over the ice is still about 1 K warmer compared to the 10 yr average before. That anomaly cannot be related to warm air advection as during winter, because SLP anomalies cannot support such an argument. Instead, the T2M warming must be influenced by a reduced sea ice thickness as a result of the warm winter atmosphere. Thickness is reduced almost all over the ocean with values around −30 cm in the central Arctic and maximum values of −70 cm. SIC is distinctly negative at the ice margin of the Barents Sea and the Beaufort Sea coast, but only slightly negative away from the margins. Again, SST anomalies are roughly following the SIC.

During summer (JAS, AVD, Fig. 3a, third row), sea ice concentration (SIC, here expressed by September conditions) is reduced all over the place with maximum amplitudes of −0.4 in the central Arctic. This picture is the result of the 30-case-averaging procedure in which individual cases would show reduced ice only in different sectors. The procedure results in small average reductions at the margins. A generally retracting

OSD
9, 2327–2373, 2012

R. Döscher and T. Koenigk

ice cover during the 100-yr-long model runs is also contributing to the only modest average reduction values at the margin, as RILEs are increasingly occurring in the more central areas. SST warming again is following the pattern of SIC. Atmospheric surface temperature (T2M) is only slightly increased during summer in ice margin areas (coastal Beaufort Sea and north of Spitsbergen) , which are about consistent with a high number of ice free summers among the 30 events in those areas. Over the remaining ice, T2M is close to the freezing point.

The SLP anomaly during the summer event is given by an elongated high pressure ridge over the European and Eurasian coast, connected to an anomalous inflow of warm air from the Nordic Seas into the Arctic ocean. This is completely different compared to the externally controlled cases as illustrated in Fig. 2, indicating influence of internal processes. Consequences of that average SLP anomaly on other average anomaly fields such as thickness or shape of ice cover cannot be detected here. However, a similar pattern is found in composites of specific events with least extreme SIC reductions and least extreme winter warming, both connected to rather moderate loss events of summer sea ice extent (no figure), indicating a role of this SLP anomaly pattern for modest loss events rather than for the most extreme events.

Summer sea ice thickness (in Fig. 3a expressed by September conditions) is reduced by up to 45 cm. Areas of biggest average thinning are not completely identical with areas of strongest ice concentration reductions, indicating non-linearities due to different mechanisms involved in the individual events, and due to very thick ice at parts of the Siberian coast. Case studies (Sect. 4.5) and composite analysis (Sect. 4.4), which explore individual events or groups of events, both show a better coherence between reductions of thickness and concentration.

Bottom melting during spring and summer (Fig. 3c) is increased in large areas. Strongest melt rates are seen in those areas with strongest reduction of sea ice concentration. Increased heat absorption through leads affects water temperature underneath the ice, which in turn leads to stronger melting.

During fall (OND, Fig. 3a), T2M over sea ice is much warmer than the average 10 yr before (up to 3–4 K). Anomalous atmospheric circulation can only support a part of that warming of the central Arctic by advection from the Nordic Seas. Due to the clear limitation of the strongest warming pattern to the ocean, a much reduced SIC and a diminished ice thickness must be the major reason for the warm air anomaly. Reduced ice concentration and thickness during the last three months of the year is consistent with the view of a later start of the freezing season with subsequently less dense and thinner ice cover. Similar effects have been observed after low-ice summers after year 2000 (Overland and Wang, 2010)

The average winter (JFM, Fig. 3b) after a summer event still shows anomalously warm T2M over all the Arctic ocean, but the signal is smaller and more localized than during the foregone fall. SIC is largely back to normal with slightly increased concentration in the Greenland Sea, indicating a recovery of sea ice extent above the 10 yr reference period. Ice thickness is still below normal away from the Nordic Sea ice margins. This can potentially contribute to the still warmer T2M, but horizontal patterns do not coincide well. Instead the winter T2M anomaly is reminiscent of the previous fall SIC anomaly pattern, indicating a signal storage in the ocean surface temperature. SLP shows a low pressure anomaly over large parts of the Arctic and Nordic Sea area. The pattern is reminiscent of the positive phase of the Arctic Oscillation. The specific shaping tends to decouple the Arctic from the Pacific sector circulation, but in other sectors allow for advective warming from southern latitudes, thus contributing to the T2M anomalies.

The following spring (AMJ, Fig. 3b) shows only minor anomalies for T2m and SLP. Sea ice thickness anomalies show persistence with thinner ice at the Siberian coast and in the Arctic interior (the transpolar drift area) compared to the reference period. Thinning of more than 10 cm can be considered exceeding the long-term trend. . The same is true for the following summer (JAS, Fig. 3b), which in addition shows a recovered sea ice extent due to increased SIC compared to the summer before. Still the summer SIC is locally much lower than the 10-yr reference period.

During the following fall (OND, Fig. 3a) T2M over the Arctic ocean is still anomalously warm over the ice, likely due to ice concentrations or ice thickness which are still below normal in the Arctic interior. SLP anomalies do rather not support advective influences.

Reviewing the average development of the ice field, we see only slightly reduced SIC during the average winter (JFM) of the event year. During the event summer, maximum reduction is reached. This is maintained even during the fall directly after the summer event. The following winter, spring and summer show only moderately negative SIC anomalies away from the ice margin. The interior ice thickness anomaly remains strongly negative during the complete two-year-period. Despite the only moderately negative SIC anomalies during the year after the event, we still find a strongly positive T2M anomaly during the second fall after the summer minimum event. Thus the T2M fall anomaly is reoccurring after a spring and a summer without relevant T2M anomalies, while the sea ice extent and concentration are clearly recovering. As the fall T2M anomaly is largely limited to the ice-covered ocean area, its survival must be due to a signal storage mechanisms related to sea ice or ocean. In the winter after the event we see effects of a warmer ocean underneath the ice. For the year after the summer minimum, Blanchard et al. (2011) suggest a re-occurrence by means of memory in the ice thickness, which has an annual or even longer time scale. We see no other mechanism that could be responsible for the re-occurence. Accordingly, we suggest that the fall T2m signal reemerges because of the still anomalous ice thickness.

4.3 The role of the Arctic Dipole (AD) anomaly

To find dominant modes of sea level pressure (SLP) variability over the Arctic, we calculate EOFs based on winter (JFM) means north of 70° N for the complete analysis period 1980–2079. A typical result is shown for scenario E1 (Fig. 4). The first EOF with a center over the Arctic ocean is dominating the variability with an explained variance of 59 % and represents the Arctic Oscillation (AO). The second EOF mode with an explained variance of 15 % shows an almost straight neutral (zero) line over the pole, and represents the Arctic Dipole Anomaly (DA) similar to Wu et al. (2006). Centers of

OSD
9, 2327–2373, 2012

R. Döscher and T. Koenigk

oscillation are located over North America and Siberia. The third mode with a smaller explained variability of 9 % is rotated by about 90° compared to the DA. (As an alternative definition based on larger SLP fields between 10° N and 90° N, the DA would result as the third principal component after AO/NAO and the Pacific North America anomaly PNA, Overland and Wang, 2010). The associated principal component time series show no significant long term trends, but annual-decadal variability. The distribution of the DA mode amplitudes for all 6 scenario experiments (Fig. 5, upper panel) shows a slightly skewed distribution with a maximum towards positive values. When selecting only the most extreme sea ice reduction events (Fig. 5, mid panel), we see exclusively positive amplitudes for the DA mode, while the leading AO mode and the nameless third EOF mode give both negative and positive amplitudes. The opposite selection of the remaining reduction events give both negative and positive amplitudes for all three modes. Thus the most extreme rapid sea ice loss events are connected to positive DA anomalies during the winter before, which implies atmospheric warm inflow of Pacific origin into the Arctic. This finding is concordant with 2d composite results for the 20 % most extreme cases (COMP, Fig. 6c), also indicating increased atmospheric inflow from the Pacific sector.

It becomes clear that the most extreme cases of sea ice extent drop require a positive DA phase. In reverse however, a positive DA phase does not guarantee a summer sea ice drop. Thus, a positive DA is a necessary, but not a sufficient condition for an extreme sea ice extent drop. This is again an expression of the role of meridionality for rapid change events.

Viewing the principal component time series in the example of Fig. 4e, the DA amplitude is subject to interannual as well as to clearly visible interdecadal variability. Low phases are preventing strong extreme events.

4.4 Composites

To find out more about the major mechanisms connected to extreme sea ice events, we build composites based on selected members of the 30-member ensemble of rapid

OSD
9, 2327–2373, 2012

sea ice loss events. Selection criteria are chosen to cover the 20 % (6 out of 30 events) respective most extreme events. We define composites based on either summer (of the event) or winter (the winter before the event) conditions, and show resulting patterns for both winter and summer. Table 2 summarizes the different composites.

The composites #1 and #2 are defined by a warm resp. cold winter (JFM) 2-m-air temperatures in comparison to the 10-yr reference period. Composite #1 covers air temperature anomalies greater than 3.85 K, corresponding to the six warmest cases. Fig. 6a shows the warming pattern which is connected to strongest anomalies of summer sea ice concentration and summer extent (-2744×10^3 km^2, see Table 1 for sea ice extent). This is even true for summer thickness (no figure). The winter SLP pattern supports advection of warm air into the Arctic from both the Atlantic sector, from eastern Europe and from the American west coast. In reverse, cold winters (composite #2, no figure) give moderate summer sea ice concentration reductions, connected with an isolating low pressure anomaly over the central Arctic. The reason why these cases still show a moderate rapid change event during summer, are to be found during summer itself ("summer-driven cases") when the SLP patterns like the one in Fig. 3a ("summer SLP") supports advection of warm air from the Atlantic. Those summer SLP conditions are in general agreement with the 30-case-average description in section TWOD. Ice extent event values can be less than the original selection criterion of the event definition (1200×10^3 km^2) because the numbers here refer to average year-to-year changes, while the event definition covers the cumulative effect of up to 3 yr.

Small negative concentration anomalies at the ice margins in Fig. 6 might be counter-intuitive but can be explained by small concentrations even during the reference period directly before the event (which might be anywhere on the scenario time axis), and by spatially-different ice-free areas among the members of the composite.

Both strong and weak concentration anomalies occur during sea ice reduction events. Composite #3 is defined by the lowest spatial-average September sea ice concentrations compared to the reference period ("d_SIC < −0.1336"). Those concentration anomalies (Fig. 6b) are most negative on spatial average. Locally, other composites can show stronger reductions. This composite is connected to a strong extent reduction (Table 2), slightly smaller ($\sim 400 \times 10^3$ km^2) than the most extreme composite. For this composite we find a winter SLP anomaly pattern quite similar to the "T2M > 3.85 K" composite, indicating that winter atmospheric warming by atmospheric circulation indeed plays a major role for the most extreme summer sea ice concentrations.

Composite #4 collects the most extreme drops of summer sea ice extent. Those drops ("d_extent < -2417×10^3 km^2", Fig. 6c) occur in connection with an air inflow anomaly from the Nordic Seas during summer and a surface air temperature anomaly over the ice during the winter before the event. The summer atmospheric circulation anomaly is caused by a low pressure anomaly over Greenland and high anomalies over the Bering Sea and Kara Sea. It is the Kara Sea summer SLP anomaly pattern that dominates the all-event average during summer (Fig. 3a).

The winter SLP anomaly shows a tripod-like pattern with a low anomaly over the eastern Arctic and three high pressure anomalies over southern Siberia, the Nordic Seas and Alaska. The pattern consisting of the Alaska high and the central low anomaly bears some resemblance of the Arctic Dipole Anomaly (DA) pattern (Wu et al., 2006) in its positive phase. Both positive DA and the tripole seen here are suitable to foster atmospheric inflow from the Pacific area into the Arctic. EOF analysis in section XX shows that indeed a strong positive state of DA oscillation is a necessary constituent for an extreme RILE. It is the tripod-like winter SLP anomaly pattern which dominates the all-event-winter-average (Fig. 3a). In addition to the pure DA pattern, it brings warm air from the Pacific to the Arctic. An associated sea ice thinning (no figure) is centered in the Chukchi Sea and shows a horizontal pattern similar to the atmospheric warming anomaly.

Composite #5 (Fig. 6e) collects the most extreme cases in terms of summer sea ice export anomaly through Fram Strait. The strongest cases ("strong export") are connected to a winter SLP anomaly suited to transport ice from the Beaufort Sea towards Fram Straits. This winter pattern is in agreement with a positive AO index. During

OSD
9, 2327–2373, 2012

summer, the "strong export" case is connected to a large scale SLP anomaly pattern with a low over the Norwegian and Barents Sea and a high over the western Arctic, indicating an atmospheric forcing of sea ice movement towards Fram Straits. In the opposite case ("weak export", #6), events are connected to negative export anomaly, which is connected to a large scale SLP pattern of opposite polarity suitable to hamper ice export.

Interestingly, the weak export composite #6 gives a stronger RILE than the export composite. This is due to anomalous advection of warm air into the Arctic during summer, due to the pressure anomaly pattern. The warming effect is out-competing the effect of ice transport. The event amplitudes ($2008 \times 10^3\,\mathrm{km}^2$ for the weak export and $1333 \times 10^3\,\mathrm{km}^2$ for the strong export) both show moderately strong events. This indicates that the strength of sea ice export itself is not an important factor for generating rapid sea ice reductions in our model.

An additional composite pair (no figure) distinguishes one-step cases from two-step cases (see definition of events). Interestingly, the one-step composite gives figures very similar to the weak export case (composite #6), confirming that strong single-step events require the summer inflow from the Atlantic sector. Two-step events are more dependet on the winter atmospheric circulation with SLP anomalies very similar to the strongest events in composites #1 and #4 .

Table 2 summarizes the composites. The relation between September SIC and strength of the event is quite linear. As to be expected, the event strength increases both with winter and summer T2m. Note that the combination of warmest T2M anomalies for winter and September (composite #1) leads to a strong event, but is outrivaled by a combination of more moderate (but still strong) T2m anomalies (composite #4), pointing to influences of more detailed flow patterns and other effects.

4.5 Individual cases

To further assess mechanisms behind rapid reduction events, we also need to explore individual cases. With our definition of a rapid reduction event, we cover strong

OSD
9, 2327–2373, 2012

R. Döscher and T. Koenigk

one-step events as well as events in several steps, i.e. involving a series of consecutive ice reductions from summer to summer. Most cases involve more than one step.

For further examination, here we choose case 1 (with reduced ice in the Pacific and Atlantic sectors), case 16 (with reduced sea ice off the Eurasian and Alaska coast), and case 26 (with reduced sea ice cover off northern Canada during summer). Anomalies in this section are referring to the difference between a specific season and the corresponding 10-yr average season directly before the event. If the case is a multiple-step event, the 10 yr reference period ends at the beginning of the first step.

Case 1 with a sea ice record minimum during summer 1998 is a one-step event in the ice extent. A sequence with seasonal means starting two winters before the summer event are shown in Fig. 7.

The two preceding winters before the summer event both show anomalously warm atmospheric conditions over parts of the Arctic ocean. In both winters, the warm surface temperatures can be associated with atmospheric transport anomalies as inferred from SLP anomaly patterns. This is even true for the two falls before those winters. This leads to generally thinner ice compared to the 10 yr average reference period. The sea ice thickness anomaly shows first signatures of the 1998 event already during the summer 1997. An elongated low pressure anomaly centered over the pole is connected to ice drift away from the Chukchi Sea towards the Canada Basin. The resulting thickness anomaly pattern with thinner ice in the Chukchi and Beaufort Seas remains until the event summer. T2m anomalies over the Chukchi Sea during fall 1997 and winter 1997/1998 reflect the reduced ice thickness, but are even supported by inflow of warm air from the Pacific and Siberia. This corresponds to a high amplitude of the winter AD anomaly pattern (amplitude 371). Thus, an important precondition in the winter before the summer event is fulfilled.

During spring 1998, the thickness anomaly is reflected by a generally warmer T2M over the Arctic ocean, connected with a low pressure anomaly over the same area. This SLP effect during spring is consistent with observations, linear theory and and earlier model results. The geopotential height field should display a baroclinic response with a

OSD
9, 2327–2373, 2012
Arctic rapid sea ice loss events
R. Döscher and T. Koenigk

shallow low close to the warm anomaly (Walter et al., 2001). Alexander et al. (2004) find a local and direct baroclinic response to sea ice retraction connected to near-surface warming and below-normal sea level pressure.

During the event summer, a low pressure anomaly is concentrated in the Canada Basin and northern Greenland area (similar to the average event summer, Fig. 3a), connected with atmospheric inflow from the Nordic Seas. The latter reduces sea ice concentration north of Laptev Sea. Both spring and summer 1998 show increased bottom melting (no figure). The fall and winter after the event show increased warming over large ocean and land areas. This warming reoccurs next fall due to still reduced ice thickness.

Summarizing, a generally thin ice already during 1997, assisted by an additional circulation-driven thinning during summer 1997 provided the preconditions for the 1998 event. The 1997 summer anomaly in the ice thickness survived the winter due to favorite meridional atmospheric circulation and was enhanced during summer 1998 by anomalous meridional atmospheric flow from the Atlantic sector.

Case 16 is a three-step event with a first drop of ice extent in summer 2031 following several decades of smaller variability. A large step in 2032 is followed by an additional smaller final drop in 2033.

Similar to case 1, the falls and winters before the summer drop show positive T2M anomalies over the Chukchi and Siberian Seas, which can be explained by regionally meridional atmospheric advection. Due to those repeated fall and winter conditions, initial negative ice thickness anomalies in the Chukchi and Siberian Seas survive and further develop all the way to the summer 2033. Two winters before the event (Fig. 8) show positive DA amplitudes, whereby the winter 2031/2032 shows the strongest DA value. Again and similar to case 1, an important precondition of strong meridionality (Sect. DA) during winters of the multi-step event is given. During the event summer, a high pressure anomaly centered over Bering Strait presses ice towards the coasts of Canada and Greenland.

In line with the other cases, springs during this event are often characterized by low SLP anomalies in the central Arctic, connected to anomalously thin ice.

During the summers (2032 and 2033), bottom melting is clearly compared to the 10 yr average before the events. In principle this could be either due to reduced ice concentration and associated local water heating from the surface, or due to deeper ocean influences. To examine those possibilities, we explore the spring and summer 2032, which shows a distinct positive SST (no figure) and negative ice concentration anomaly (Fig. Case16) in the Chukchi and East Siberian Seas.

Winds drive away the ice from and Chukchi Sea. Open waters occur, connected to immediate SST warming. A zone of increased bottom melting extends about 3 grid boxes (about 150 km) under the ice and leads to additional ice concentration reduction until the wind driving stops. In that area of mixed ice and open water within individual grid boxes, the fraction of open water and bottom melting increases simultaneously. After an initial reduction of ice concentration, heat is absorbed by the upper ocean layer and immediately used for bottom melting, such that SST is not increasing for some time. In the given example we see a time delay of about 10 days between ice fraction opening and SST response A mechanism similar in principle has been observed during the 2007 event by Perovich et al. (2008).

We also tested the idea of possible upward transport of ocean heat by vertical mixing in response to reduced ice concentration. No sign of such a process was found in this model. We find locally increased vertical mixing at grid points with strongly reduced ice concentration, reaching down to several tens of meters, but the heat source is the surface, not the ocean.

Case 26 is a one-step event with a record sea ice extent minimum in 2025 after several decades of smaller variability on top of a downward trend. The actual event is largely driven during spring and summer 2025, but the story of case 26 starts already two winters before the actual summer event (Fig. 9). Large scale wind fields advect warm air from an anomalously warm Siberia over the Laptev Sea and give rise to a local ice thinning. This ice anomaly can now potentially survive the coming seasons

OSD
9, 2327–2373, 2012

R. Döscher and T. Koenigk

if the atmospheric and oceanic conditions allow. The initial sea ice thickness anomaly persists until the record ice extent event and is joining up on the way (during fall and winter before the summer event) with an additional ice thickness anomaly off Canada, even that one generated by anomalous meridional winds from the south. The winter before the summer event shows a moderately positive AD amplitude which potentially helps keeping the initial anomaly with winds from the Pacific almost parallel to the Canada coast. A few months later, during spring before the event summer, both initial sea ice anomalies grow. During summer, this leads to large areas of open water and low ice concentrations off the Canadian and northern Greenland coast reaching all the way to the Laptev sea, with ice remaining between the eastern Siberian coast and the pole.

Thus, an important period for this event is the spring 2025, just a few months before the record summer. Increased spring thinning off Canada is related to an atmospheric low pressure anomaly covering the Beaufort Sea, the Bering Sea and larger coastal parts of Alaska and Canada. That anomalous atmospheric circulation pushes the ice away from the coast towards the pole area, without suppressing the initial Laptev ice anomaly. A surface warming occurs as a consequence of ice retreat. This in turn supports the further existence of the atmospheric low pressure anomaly, thereby potentially constituting a positive feedback. The summer shows the typical positive SLP anomaly (as seen in in 30-case average in Fig. 3a) over the Eurasian coast in a strong realization.

Already during spring 2025, both bottom melting and surface melting increase compared the 10-yr reference period, whereby bottom melting is increasing more than surface melting. During the event summer, bottom melting is still increased due to heat entering the ocean leads.

We see an event which is preconditioned by early sea ice anomalies in the seasons before and later maintained by supportive wind patterns. The start signal of the actual event year is given in spring with opening up coastal areas and continued by strong air inflow from the Atlantic sector. This event is mainly driven by spring and summer

OSD
9, 2327–2373, 2012

R. Döscher and T. Koenigk

atmospheric forcing. Also during spring we see a self-supporting low pressure anomaly which stabilizes ice melting and offshore ice transports. Large scale circulation sets the stage for shaping the conditions for a strong ice loss event, but a local feedback contributes to the amplitude and shape of the ice extent drop.

Reviewing our three cases (cases 1, 16, 26), we find rapid ice change events with low ice concentrations in different parts of the Arctic ocean. Each event is preconditioned by an initial sea ice thinning generated by an atmospheric circulation anomaly, often connected with northward transport of heat. Depending on the atmospheric conditions of the forthcoming seasons, the anomaly survives and grows during a period of 1–3 yr, modified by wind conditions and partly regional feedbacks. Events can be dominated both from preconditioning or from summer atmospheric forcing conditions. After the event summer, atmospheric conditions favor a less meridional circulation leading to a partial recovery of sea ice. This is also found e.g. in the composite #4 of the most extreme events which gives a stronger SLP-anomaly-isolation over the ocean during the winter of recovery (no figure).

Each event is connected to increased bottom melting during the summer. The increased bottom melting is explained by large lead areas where atmospheric heat can be absorbed by the uppermost ocean layer and thereby contribute to bottom melting. We see no indication for a bottom melting initiated by large scale heat fluxes in the ocean. Furthermore, we see no sign for decisive impact of radiative fluxes on triggering ice events. Long wave radiation anomalies are merely reflecting surface air temperature changes. Short wave solar radiation does not play a major role for generating the sea ice events in our model simulations. In the example of case 16 we see that the long wave downward radiation (no figure) hitting the surface is strongly reflecting T2M anomalies, which often are strongly positive over thinning ice, but is also affected by warmer air of southern origin appearing over the areas during winter. Anomaly patterns of short wave downward radiation give only vague indication for a direct solar impact on the sea ice events. It appears hard to find examples of decisive influence of short wave downward radiation. In case 1, an extra solar downward radiation of less than

OSD
9, 2327–2373, 2012

5 W m^{-2} is seen during the spring in regions with strongly reduced ice during the coming summer. No corresponding signal in cloud cover can be found, and surface melting is rather reduced. Thus, radiative changes play a minor role in our cases. However it should be noted that this finding is based seasonal means.

In most cases (case 1 and 26), a warm air anomaly in spring is connected to a low pressure anomaly. In at least one case (case 26) we see indication for localized positive feedback between thin ice, connected to high surface air temperatures and a low pressure anomaly, which supports advection of new warm air into the area of thin ice. This is a self-supporting mechanism that helps keeping or strengthening the initial thickness anomaly. Warm air anomalies during winter are generally not connected to low pressure anomalies at the surface. Fall and winter are more constrained by the large scale circulation. In this study, we are limited to surface variables. However the situation might look different for higher atmospheric levels. Overland an Wang (2010) show in a reanalysis-based study that sea ice reduction and warmer surface during fall leads to direct baroclinic signals e.g. in the the 1000–500 hPa thickness field, while barotropic signals are more variable and thus not necessarily visible for the sea level pressure (SLP) fields in monthly or seasonal means.

Positive DA anomalies, identified here as a necessary but not sufficient winter preconditions for very strong events, clearly helps in all three cases. All cases show positive DA anomalies, whereby two stronger ones are involved. Case 16 illustrates, that a moderately positive DA supports the development towards the event, but the creation of the initial thickness signal is not connected to the DA.

5 Summary and discussion

We use a mini-ensemble of 6 different numerical Arctic climate scenario experiments each of 100 yr length to investigate a total of 30 rapid sea ice loss events.

Summer sea ice extent decreases with time and the likelihood of a rapid sea ice loss event increases with time and thus with thinning ice and reduced ice extent. In

OSD
9, 2327–2373, 2012

addition to the general trend of of summer sea ice extent, we see decadal variability in all runs. Different variability timing within the ensemble would point towards pure local Arctic self-contained mechanisms (Döscher et al., 2009). However, we find similar interannual and interdecadal variability of summer sea ice among ensemble members. Thus, summer ice extent is partly governed by global-scale atmospheric circulation, which is enforced by lateral atmospheric boundary conditions (at the outer boundary of the regional model domain) identical to all regional runs. In addition to common variability, we see clustering of RILEs during certain periods in the different scenario experiments. Large scale atmospheric circulation supportive in reducing thick ice off the Siberian coast, provides a strong potential for a RILE, so that many ensemble members actually generate events.

In our model, ice in the Siberian Sea tends to be artificially thick as a result of insufficient treatment of ice classes (Mårtensson et al., 2012) and likely due to a high pressure bias over the Eurasian part of the Arctic ocean. This problem is shared with several GCMs (e.g. Vancoppenolle, 2008; Blanchard et al., 2011). Thus, results of this paper might help interpreting GCMs. Given that the artificially thick Siberian ice blocks rapid ice loss events under atmospheric circulation regimes which do not oppose that exaggerated thickness, it might be speculated that a more realistic geographical ice thickness distribution could lead to even more frequent rapid ice loss events in our model. Those might be less clustered within the ensemble. Our event case 26, timed during 2025, features a strong ice reduction off northern Greenland and northern Canada connected to ice drift away from those coasts. In such a situation, a generally thinner ice off eastern Siberia can potentially lead to an even stronger event coming close to zero sea ice during summer. Thus, almost ice free summers could be possible even before 2040. In reverse and generally spoken: specific geographical thickness distributions compensate for atmospheric forcing which potentially could generate a rapid loss event.

A RILE in the given climate change experiments can be evoked by specific forcing conditions applied on the sea ice during the winter before the summer event, or

OSD
9, 2327–2373, 2012

by spring and summer atmospheric forcing. Winter conditions are preconditioning the coming summer, but not necessarily leading to an ice reduction event.

On average, rapid reduction events are characterized by increased temperatures over the ice during the winter before a summer event. Warmer air temperatures are caused by atmospheric circulation anomalies and impede sea ice growth, thus leading to less-than-average thickness already during that winter, whereby the average is represented by the respective 10 yr average before the start of the event year. Average spring temperature warm anomalies are related to the reduced ice thickness. Average summer conditions feature a high pressure anomaly along the Eurasian coast, and a slight negative anomaly over Greenland and the northern Canada coast, balancing an anomalous atmospheric inflow from the Nordic Seas into the Arctic. The average summer event shows even increased melting at the bottom of the ice. Those average conditions give a very general picture because individual cases vary in mechanism and geographical location.

Studies of specific cases show that a winter thickness anomaly can already be preexisting in the winter before the summer event. In those cases, the atmospheric conditions during the year before are responsible for the initial thinning.

Composites of specific atmosphere and sea ice conditions reveal that the most extreme drops in sea ice extent occur in the combined case of winter atmosphere warming and a summer cyclonic anomaly between the pole and Greenland. That summer low anomaly is accompanied by high-pressure anomaly over the Kara Sea connected to inflow of air from the Nordic Seas into the central Arctic, and by a high-pressure anomalies over Alaska which turns the anomaly flow towards the northern Canada coast. More moderate RILE cases only show the Kara Sea summer anomaly.

The winter warming in extreme cases is supported by atmospheric inflow from the Pacific area. This is affirmed by an EOF analysis showing exclusively positive amplitudes for the DA anomaly (defined as the 2nd EOF of seasonal mean SLP north of 70° N) for the most extreme drop cases, meaning increased pressure over North America and Greenland combined with reduced pressure over northern Eurasia. We

OSD
9, 2327–2373, 2012

conclude that the most extreme sea ice drops are not possible without a positive DA phase during winter. Analysis of observed sea ice reduction events point in the same direction: Wang et al. (2009) find record lows of Arctic summer sea ice extent to be triggered by the DA pattern. Observations also show a shift from largely zonal AO SLP patterns over the Arctic towards more DA-like meridional circulation patterns after the millenium shift (Zhang et al., 2008). Reanalysis data sets show interannual and multi-annual variability of oscillation patterns in the Arctic (Overland and Wang, 2005). Concluding, decadal variability of the DA such as found in our model is a near-realistic feature and thus our runs suggests the possibility of alternating intensity of ice loss events in the future.

The only observed reference for our simulated RILEs is the 2007 sea ice record minimum event (e.g. Stroeve et al., 2008). As outlined in the introduction, atmospheric circulation anomalies dominated the event which was preconditioned by anomalously young and likely thin ice. The observed summer SLP pattern of below-normal pressure over Siberia and Laptev Sea and above-normal pressure over the western Beaufort Sea and northern Canada corresponds to the strongly meridional flow carrying heat from subpolar latitudes (Ogi et al., 2008). Those factors in modified shape are shown to play a vital role in the simulated events of our model, even if the polarity is different from the specific year 2007. Kauker et al. (2009) show that winter preconditioning played a vital role for the 2007 event. In our model, that preconditioning is realized through warm winters by means of large scale circulation anomalies.

Besides the DA, another expression of high pressure over northern Canada and the Beaufort Sea is the positive phase of the PNA, a wave train anomaly covering the North Pacific and the North-American west coast. In observations, both patterns (DA and PNA) are not correlated (e.g. Overland et al., 2008). Thus oscillations of the PNA can potentially support or damp the amplitude of the DA which represents an important RILE forcing.

After the lowest sea ice extent is reached in an event, the following years show recovery of varying amplitude, characterized by a lack of the conditions mentioned above. I.e. winters are not much warmer than the respective 10 yr reference period and atmospheric circulation shows only moderate meridional components. Ice thickness anomalies as created during the event, do not predetermine a continued reduction of summer extent.

The fact that we do not see a complete sea ice removal down to almost zero before 2040 in our model, could in principle be explained either by time limitation of supporting random winter and summer forcing conditions, which coincidentally do no occur more than 1–3 yr in a row, or by negative feedback mechanisms. A summer with little sea ice is always followed by a warm fall, and sea ice thickness anomalies can persist for several seasons. This gives a strong potential for another low-ice season the coming summer. That potential is used e.g. in our simulated multi-step events, but it ceases mostly within 1–3 yr. Events longer that 3 yr are rare. In other cases, atmospheric circulation conditions do not support a further ice reduction, and thus, regular Arctic cooling mechanisms such as longwave upward radiation in combination with a less meridional atmospheric flow becomes the dominant influence. Reasons for a more zonal circulation after the events might be a response to the anomalously warm Arctic. A reduced meridional temperature gradient, connected to reduced cyclonic activity in subpolar regions is suitable to reconstitute the large scale dynamic isolation of the Arctic. From the existence of both multi-year events and single-year events in our experiments we can conclude that no systematically dominating seasonal negative feedback exists in our model.

Recovery after ice reduction is also seen regularly in the observed record of summer sea ice extent since 1979 (Stroeve et al., 2008). The ability of the sea ice to recover has also been demonstrated by Tietsche et al. (2011). A GCM is perturbed by complete removals of sea ice during summer. The response is a recovery back to the centennial trend due to compensating mechanisms such as increased heat loss at the top of the atmosphere and decreased heat gain by atmospheric advection from lower latitudes. Such seasonal negative responses or compensating mechanisms out-compete the positive feddbacks such as the sea ice albedo feedback.

Our model shows no specific role of sea ice export for rapid change events. Cases of most intense export rates are not related to strongest amplitude of summer sea ice loss. Even compared to recent observed conditions, this is not an odd result: Stroeve et al. (2008) find that loss of old ice in the 1990s was accentuated by anomalous wind patterns that led to increased ice export through Fram Strait, while recent loss in the central Arctic is due to old ice failing to survive within the Arctic ocean. Koenigk et al. (2006) found in a GCM-based study that Arctic sea ice volume is generally weakly correlated with export on interannual time scales.

Climate models have different deficiencies in describing sea ice processes. Despite problems, mechanisms are at work leading to interannual variability of sea ice conditions. The mechanisms for rapid ice loss we find here are predominantly related to atmospheric circulation and seasonal-to interannual memory build up in the ice thickness. We also tested the idea of possible upward transport of ocean heat by vertical mixing in response to reduced ice concentration. Such a process was not found in this model although observations indicate import of warm ocean water from the Pacific Ocean (Woodgate, 2010) and proximate inclusion in vertical mixing. While those observed results are under discussion, we cannot expect to find them in the model due to to coarse resolution and insufficient Bering Strait inflow. Further observational studies indicate the possibility of contributions from temporarily and locally increased radiative effects (Francis and Hunter, 2006; Kay et al., 2008) or from black carbon aerosols (Shindell and Faluvegi, 2009). None of those effects play a major role in our results. Instead we find RILEs triggered by atmospheric circulation anomalies which kept going due to local anomalies of air temperature, ice thickness and bottom melting. RILEs are evoked frequently without a major contribution related to changing local radiative forcing of sea ice, other than increased absorption in response to reduced ice concentration. This finding is not contradicting observation-based result. Even in the real world, variability in the atmospheric circulation has played an especially prominent role for rapid ice loss (e.g. Serezze and Barret, 2010), while radiative effects have been questioned (Schweiger et al., 2008). Thus, the mechanisms found in this paper should

OSD
9, 2327–2373, 2012

be seen as major contributors to RILEs. Enhanced roles for other mechanisms are well possible and need to be addressed in forthcoming studies. In this paper we are studying a large number of events as a whole, as composites or a few specific cases. Mostly, we are considering seasonal means. A follow-on study by Paquin et al. (2012) is focusing on specific RILE events with a partly increased role of radiative effects for certain months and certain cases.

Preconditioning and large scale atmospheric conditions have been identified as major cause to rapid change events in this study. Prediction efforts must thus focus on just those. A prediction system will have to rely on ice observations and atmospheric prediction. Local ice thickness as well as concentration will be essential. On the atmospheric side, seasonal prediction is subject of research, but will necessarily include elements of probability, which propagate to a seasonal ice forecast system. Lessons learned from the community S4D sea ice outlook effort (e.g. Kauker et al., 2009) are compatible with our finding on predonditioning as an important element.

Acknowledgements. This work was carried out at the Rossby Centre at the Swedish Meteorological and Hydrological Institute (SMHI) and made possible by the support of the EU-DAMOCLES project and the ADSIMNOR project funded by the Swedish research council FORMAS. We further thank Ulf Hansson and Klaus Wyser and Markus Meier for contributing during the various phases of model development.

References

Alexander, M., Bhatt, U., Walsh, J., Timlin, M., Miller, J., and Scott, J.: The atmospheric response to realistic Arctic sea ice anomalies in an AGCM during winter, J. Climate, 17, 890–905, doi:10.1175/1520-0442(2004)017<0890:TARTRA>2.0.CO;2, 2004.

Blanchard-Wrigglesworth, E., Armour, K. C., Bitz, C. M., and DeWeaver, E.: Persistence and Inherent Predictability of Arctic Sea Ice in a GCM Ensemble and Observations, J. Climate, 24, 231–250, doi:10.1175/2010JCLI3775.1, 2011.

Cassano, J. J., Higgins, M. E., and Seefeldt, M. W.: Performance of the Weather Research and Forecasting Model for Month-Long Pan-Arctic Simulations, Mon. Weather Rev., 139, 3469–3488. doi:10.1175/MWR-D-10-05065.1, 2011.
Comiso, J. C., Parkinson, C. L., Gersten, R., and Stock, L.: Accelerated decline in the Arctic sea ice cover, Geophys. Res. Lett., 35, L01703, doi:10.1029/2007GL031972,2008.
Döscher, R., Wyser, K., Meier, H., Qian, M., and Redler, R.: Quantifying Arctic Contributions to Climate Predictability in a Regional Coupled Ocean-Ice-Atmosphere Model, Clim. Dynam., 34, 1157–1176, doi:10.1007/s00382-009-0567-y, 2009.
Döscher, R., Willen, U., Jones, C., Rutgersson, A., Meier, H. E. M., and Hansson, U.: The development of the coupled ocean-atmosphere model RCAO, Boreal Environ. Res., 7, 183–192, 2002.
Francis, J. A. and Hunter, E.: New Insight Into the Disappearing Arctic Sea Ice, Eos Trans. AGU, 87, 509–511, doi:10.1029/2006EO460001, 2006.
Gerdes, R. and Köberle, C.:: Comparison of Arctic sea ice thickness variability in IPCC Climate of the 20th Century experiments and in ocean – sea ice hindcasts, J. Geophys. Res., 112, C04S13, doi:10.1029/2006jc003616, 2007.
Holland, M. M., Bitz, C. M., and Tremblay, B.: Future abrupt reductions in the summer Arctic sea ice, Geophys. Res. Lett., 33, L23503, doi:10.1029/2006GL028024, 2006.
Hunke, E. C. and Dukowicz, J. K.: An elastic-viscous-plastic model for sea ice dynamics, J. Phys. Oceanogr., 27, 1849–1867, doi:10.1175/1520-0485(1997)027<1849:AEVPMF>2.0.CO;2, 1997.
Jones, C. G., Willén, U., Ullerstig, A., and Hansson, U.: The Rossby Centre Regional Atmospheric Climate Model part I: model climatology and performance for the present climate over Europe, Ambio, 33, 199–210, 2004a.
Jones, C. G., Wyser, K., Ullerstig, A., and Willén, U.: The Rossby Centre Regional Atmospheric Climate model part II: application to the Arctic climate, Ambio, 33, 211–220, 2004b.
Kauker, F., Kaminski, T., Karcher, M., Giering, R., Gerdes, R., and Voßbeck, M.: Adjoint analysis of the 2007 all time Arctic sea-ice minimum, Geophys. Res. Lett., 36, L03707, doi:10.1029/2008GL036323, 2009.
Kay, J. E., L'Ecuyer, T., Gettelman, A., Stephens, G., and O'Dell, C.: The contribution of cloud and radiation anomalies to the 2007 Arctic sea ice extent minimum, Geophys. Res. Lett., 35, L08503, doi:10.1029/2008GL033451, 2008.

Kjellström, E., Bärring, L., Gollvik, S., Hansson, U., Jones, C., Samuelsson, P., Rummukainen, M., Ullerstig, A., Willén, U., and Wyser, K.: A 140-year simulation of European climate with the new version of the Rossby Centre regional atmospheric climate model (RCA3), SMHI reports meteorology and climatology RMK No. 108, 54 pp., 2005.

Koenigk, T., Mikolajewicz, U., Haak, H., and Jungclaus, J.: Variability of Fram Strait sea ice export: causes, impacts and feedbacks in a coupled climate model, Clim. Dyn., 26, 17–34, 2006.

Koenigk, T., Döscher, R., and Nikulin, G.: Arctic future scenario experiments with a coupled regional climate model, Tellus A, 63, 69–86, doi:10.1111/j.1600-0870.2010.00474.x, 2011.

Køltzow, M.: The effect of a new snow and sea ice albedo scheme on regional climate model simulations, J. Geophys. Res., 112, D07110, doi:10.1029/2006JD007693, 2007.

Kwok, R.: Summer sea ice motion from the 18 GHz channel of AMSR-E and the exchange of sea ice between the Pacific and Atlantic sectors, Geophys. Res. Lett., 35, L03504, doi:10.1029/2007GL032692, 2008.

L'Heureux, M. L., Kumar, A., Bell, G. D., Halpert, M. S., and Higgins, R. W.: Role of the Pacific-North American (PNA) pattern in the 2007 Arctic sea ice decline, Geophys. Res. Lett., 35, L20701, doi:10.1029/2008GL035205, 2008.

Maslanik, J. A., Fowler, C., Stroeve, J., Drobot, S., Zwally, H. J., Yi, D., and Emery, W. J.: A younger, thinner Arctic ice cover: Increased potential for rapid, extensive sea ice loss, Geophys. Res. Lett., 34, L24501, doi:10.1029/2007GL032043, 2007.

Meier, H. E. M., Döscher, R., and Faxén, T.: A multiprocessor coupled ice-ocean model for the Baltic Sea: application to salt inflow, J. Geophys. Res., 108, 3273, doi:10.1029/2000JC000521, 2003.

Mårtensson, S., Meier, H. E. M., Pemberton, P., and Haapala, J.: Ridged sea ice characteristics in the Arctic from a coupled multicategory sea ice model, J. Geophys. Res., 117, C00D15, doi:10.1029/2010JC006936, 2012.

Ogi, M., Rigor, I. G.,. McPhee, M. G, and Wallace, J. M.: Summer retreat of Arctic sea ice: Role of summer winds, Geophys. Res. Lett., 35, L24701, doi:10.1029/2008GL035672, 2008.

Overland, J. E. and Wang, M.: The third Arctic climate pattern: 1930s and early 2000s, Geophys. Res. Lett., 32, L23808, doi:10.1029/2005GL024254, 2005.

Overland, J. E., Wang, M., and Salo, S.: The recent Arctic warm period, Tellus A, 60, 589–597, doi:10.1111/j.1600-0870.2008.00327.x, 2008.

OSD
9, 2327–2373, 2012

Arctic rapid sea ice loss events

R. Döscher and T. Koenigk

Overland, J. E. and Wang, M.: Large-scale atmospheric circulation changes are associated with the recent loss of Arctic sea ice, Tellus A, 62, 1–9, doi:10.1111/j.1600-0870.2009.00421.x, 2010.

Paquin, J.-P., Döscher, R., Sushama, L., and Koenigk, T.: Causes and consequences of mid-21st Century Rapid Ice Loss Events simulated by the Rossby Centre Regional Atmosphere-Ocean model, Tellus, submitted, 2012.

Perovich, D. K., Richter-Menge, J. A., Jones, K. F., and Light, B.: Sunlight, water, and ice: Extreme Arctic sea ice melt during the summer of 2007, Geophys. Res. Lett., 35, L11501, doi:10.1029/2008GL034007, 2008.

Samuelsson, P., Gollvik, S., and Ullerstig, A.: The land-surface scheme of the Rossby Centre regional atmospheric climate model (RCA3), Report in meteorology 122, SMHI, SE-601 76 Norrköping, Sweden, 2006.

Schweiger, A. J., Zhang, J., Lindsay, R. W., and Steele, M.: Did unusually sunny skies help drive the record sea ice minimum of 2007?, Geophys. Res. Lett., 35, L10503, doi:10.1029/2008GL033463, 2008.

Semtner, A, J.: A model for the thermodynamic growth of sea ice in numerical investigations of climate, J. Phys. Oceanogr., 6, 27–37, 1976.

Serreze, M. C. and Barrett, A. P.: Characteristics of the Beaufort Sea High, J. Climate, 24, 159–182, doi:10.1175/2010JCLI3636.1, 2011.

Shindell, D. and Faluvegi, G.: Climate response to regional radiative forcing during the twentieth century, Nature Geosci., 2, 294–300, doi:10.1038/ngeo473, 2009.

Steele, M., Morley, R., and Ermold, W.: PHC: A Global Ocean Hydrography with a High-Quality Arctic Ocean, J. Climate, 14, 2079–2087, doi:10.1175/1520-0442(2001)014<2079:PAGOHW>2.0.CO;2, 2001.

Stroeve, J., Serreze, M., Drobot, S., Gearhead, S., Holland, M., Maslanik, J., Meier, W., and Scambos, T.: Arctic sea ice extent plummets in 2007, Eos T. Am. G. Un., 89, 13–14, 2008.

Tietsche, S., Notz, D., Jungclaus, J. H., and Marotzke, J.: Recovery mechanisms of Arctic summer sea ice, Geophys. Res. Lett., 38, L02707, doi:10.1029/2010GL045698, 2011.

Valcke, S. and Redler, R.: OASIS4 User Guide, PRISM Technical report No.4, 64 pp., 2006.

Vancoppenolle M., Fichefet, T., Goosse, H., Bouillon,S., König Beatty, C., and Morales Maqueda, M. A.: LIM3, an advanced sea-ice model for climate simulation and operational oceanography, Mercator Ocean Quarterly Newsletter 28, 16–21, 2008.

OSD

9, 2327–2373, 2012

R. Döscher and T. Koenigk

Vinje, T.: Fram Strait Ice Fluxes and Atmospheric Circulation: 1950–2000, J. Climate, 14, 3508–3517, 2001.
Walter, K., Luksch, U., and Fraedrich, K.: A Response Climatology of Idealized Midlatitude Thermal Forcing Experiments with and without a Storm Track, J. Climate, 14, 467–484, doi:10.1175/1520-0442(2001)014<0467:ARCOIM>2.0.CO;2, 2001.
Wang, J., Zhang, J., Watanabe, E., Ikeda, M., Mizobata, K., Walsh, J. E., Bai, X., and Wu, B.: Is the dipole anomaly a major driver to record lows in Arctic summer sea ice extent?, Geophys. Res. Lett., 36, L05706, doi:10.1029/2008GL036706, 2009.
Woodgate, R. A., Weingartner, T., and Lindsay, R.: The 2007 Bering Strait Oceanic Heat Flux and anomalous Arctic Sea-ice Retreat, Geophys. Res. Lett., 37, L01602, doi:10.1029/2009GL041621, 2010.
Wu, B., Wang, J., and Walsh, J. E. : Dipole Anomaly in the Winter Arctic Atmosphere and Its Association with Sea Ice Motion, J. Climate, 19, 210–225, 2006.
Zhang, X. and Walsh, J. E.: Towards a seasonally ice-covered Arctic Ocean: Scenarios from the IPCC AR4 simulations, J. Clim., 19, 1730–1747, 2006.
Zhang, X., Sorteberg, A., Zhang, J., Gerdes, R., and Comiso, J. C.: Recent radical shifts of atmospheric circulations and rapid changes in Arctic climate system, Geophys. Res. Lett., 35, L22701, doi:10.1029/2008GL035607, 2008.

Table 1. Scenario experiments. All runs are forced by identical atmosphere forcing from ECHAM5/MPI-OM. "thickice" refers to a sea ice configuration with thicker ice (see Döscher et al., 2009, their runs 210, 211, 112, 215). "stdice" is a configuration with thinner ice "SSS restoring" refers to a sea surface salinity restoring to climatological values (see Koenigk et al., 2011).

Experiment	Description
ECH001	Ocean: PHC-winter climatol. at atlantic boundary, SSS restoring, stdice
ECH002	Ocean: PHC-winter climatol. at atlantic boundary, SSS restoring, thickice
ECH003	Ocean: PHC-winter climatol. at atlantic boundary, surface salinity flux correction, stdice
ECH004	Ocean: PHC-seasonal climatol. at atlantic boundary, SSS restoring, stdice
ECH005	Ocean: ECHAM5/MPI-OM at atlantic boundary, SSS restoring, stdice
ECH006	Ocean: ECHAM5/MPI-OM at atlantic boundary, surface salinity flux correction, stdice

OSD
9, 2327–2373, 2012

R. Döscher and T. Koenigk

Table 2. Composites as explained in the text, with columns for anomalies of 2-m-air temperature for september and winter (JFM), september sea ice concentration, and extent. Summer is defined by the three months JAS.

#	Composite description	Figure	September T2m anomaly K	Winter T2m anomaly K	September sea ice concentration anomaly (SIC)	Strength of the extent event 10^3 km^2
1	winter T2M difference >3 K	a	0.8	3.8	−0.33	−2774
2	winter T2M difference <0 K	(no figure)	0.0	−1.0	−0.1	−995
3	summer SIC difference <−0.134	b	0.7	2.9	−0.27	−2491
4	summer ice extent difference $<-2417 \times 10^6$ km^2	c	0.6	2.5	−0.3	−2937
5	summer ice export velocity anomaly >0.43 cm s^{-1}	d	0.3	1.2	−0.13	−1333
6	summer ice export velocity anomaly <−1.99 cm s^{-1}	e	0.7	0.7	−0.2	−2008

OSD
9, 2327–2373, 2012

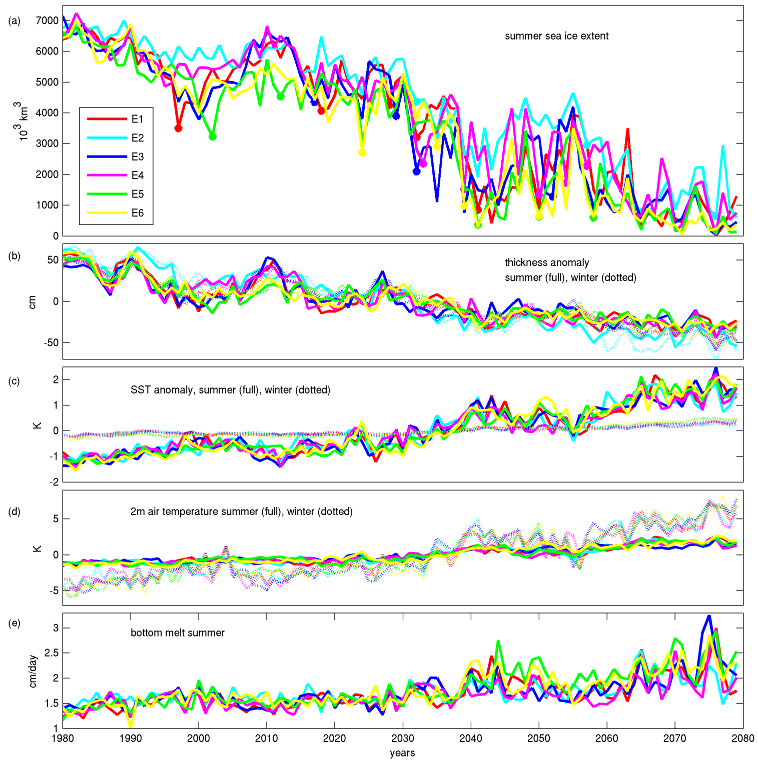

Fig. 1. Times series for six scenario experiments. **(a)** Summer (JAS) sea ice extent in 10^3 km^3, **(b)** ice thickness anomaly in cm based on concentration-weighted annual minimum ("summer") and annual maximum ("winter") sea ice thickness, **(c)** spatially averaged summer SST anomaly north of 70° N in K, **(d)** spatially averaged summer 2-m-atmospheric temperature anomaly north of 70° N in K, **(e)** ice-area-averaged summer sea ice bottom melt rate in cm day^{-1}.

OSD
9, 2327–2373, 2012

Arctic rapid sea ice loss events

R. Döscher and T. Koenigk

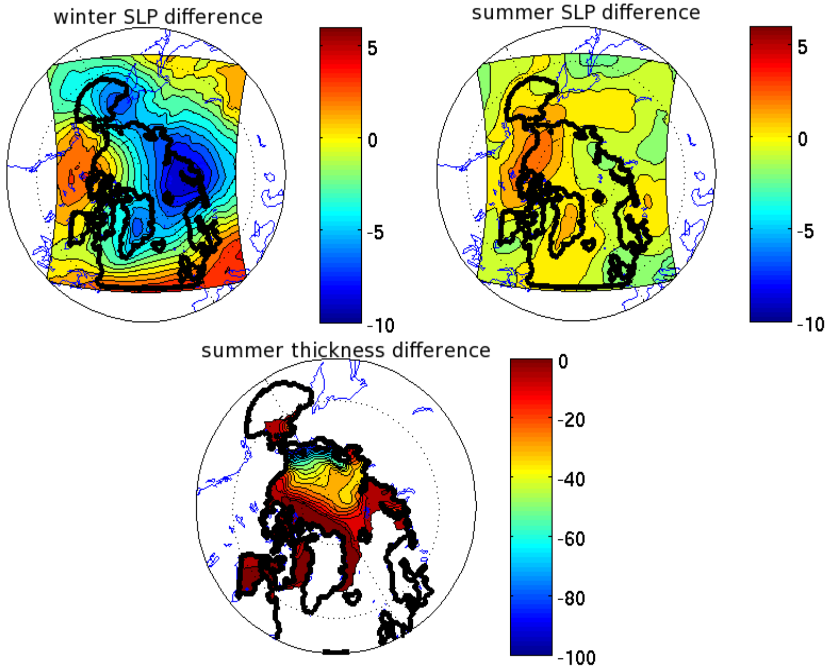

Fig. 2. Difference between RILE events 2030–2035 and the respective 10 yr mean before the events. **(a)** SLP during summer in hPa, **(b)** SLP during winter in hPa, **(c)** summer sea ice thickness in cm.

OSD
9, 2327–2373, 2012

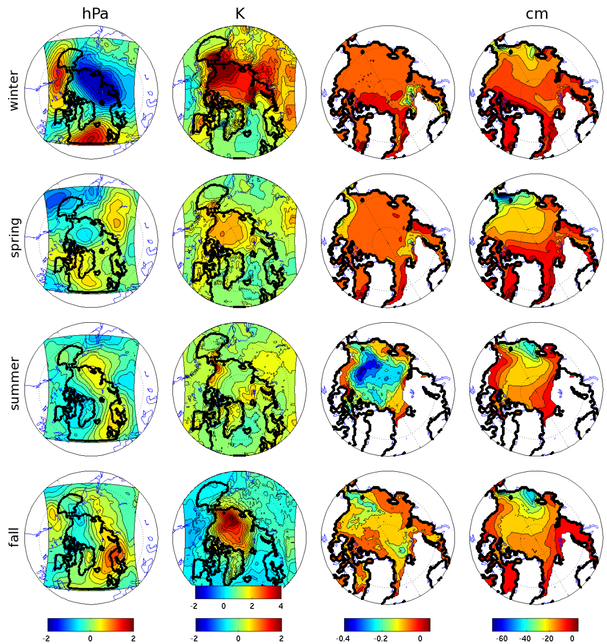

Fig. 3a. Difference between seasonal conditions during the rapid reduction event and the average conditions of the 10 yr period before the event. Winter before the event (upper row), spring before the event (2nd row), summer of the event (3rd row, SIC and thickness are represented here as September mean instead of summer mean) and fall directly after the event (lowermost row). Sea Level Pressure in hPa (left column), 2-m-air temperature in K (2nd column), SIC = sea ice concentration (3rd column) and sea ice thickness in cm (right column). Black lines represent the ocean models coastlines and boundaries. Note the different color bars for fall 2-m-air temperature.

OSD
9, 2327–2373, 2012

R. Döscher and T. Koenigk

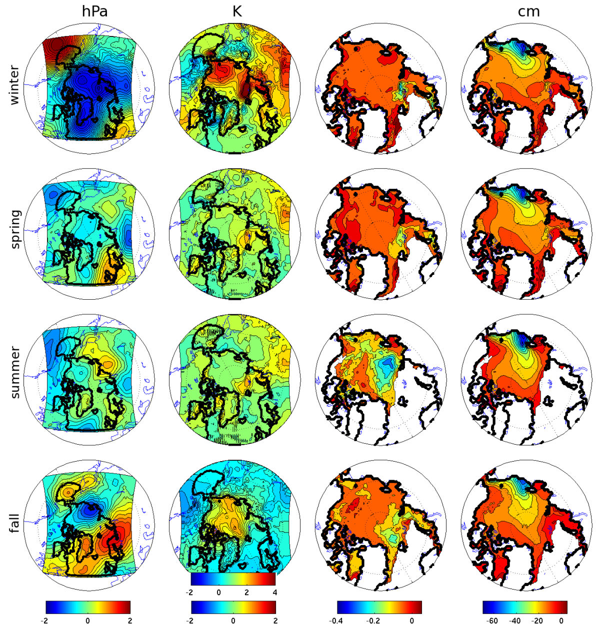

Fig. 3b. Difference between seasonal conditions of the year after the rapid reduction event and the average conditions of the 10 yr period before the event. Winter after the event (upper row), spring after the event (2nd row), summer after the event (3rd row, SIC and thickness are represented here as September mean instead of summer mean) and fall after the event (lowermost row). Sea Level Pressure in hPa (left column), 2-m-air temperature in K (2nd column), SIC = sea ice concentration (3rd column) and sea ice thickness in cm (right column). Black lines represent the ocean models coastlines and boundaries. Note the different color bars for fall 2-m-air temperature.

OSD
9, 2327–2373, 2012

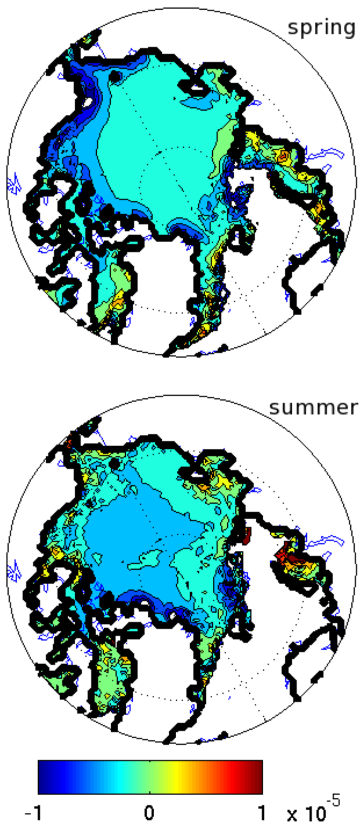

Fig. 3c. Bottom melting rate difference between seasonal conditions of the year of the rapid reduction event and the average conditions of the 10 yr period before the event. Spring (upper) and summer (lower, SIC). Negative values mean increased melting.

OSD
9, 2327–2373, 2012

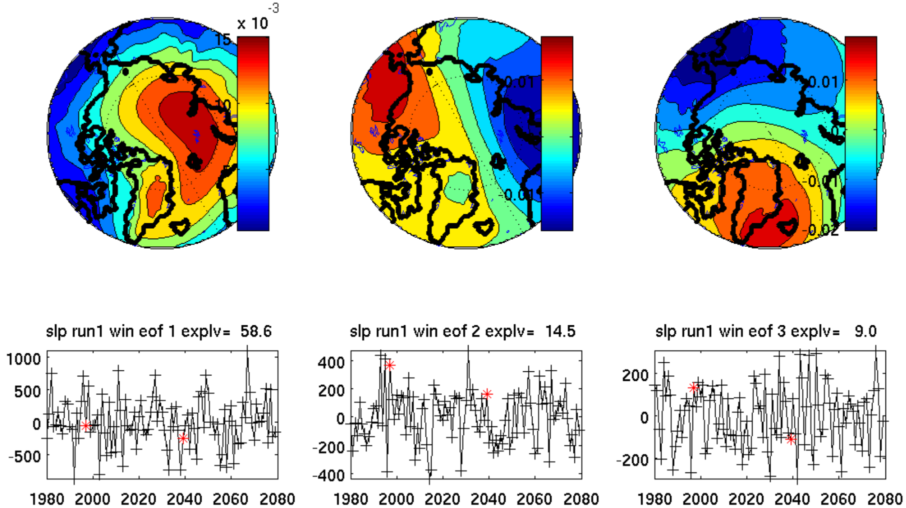

Fig. 4. EOF 1–3 of winter mean (JFM) sea ice pressure (upper panel), PC (middle panel) and probability distribution of PC amplitude (bottom panel). Red crosses indicate two out of the six most extreme rapid sea ice reduction events.

OSD
9, 2327–2373, 2012

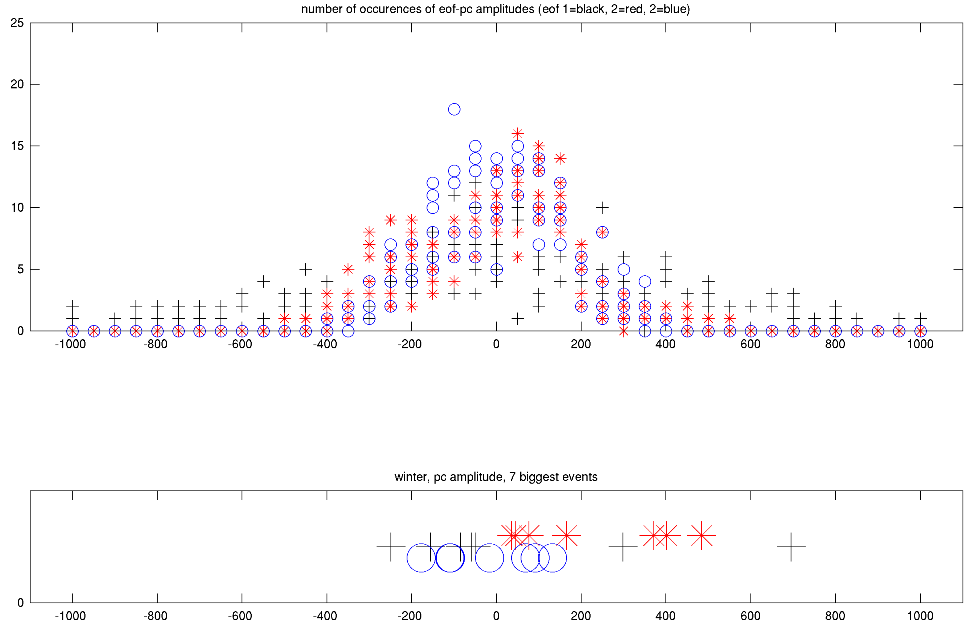

Fig. 5. Upper panel: PDF (number of occurrences) of winter (JFM) EOF-PC amplitudes (EOF1 = AO = black, 2 = DA = red, 3 = blue). Middle panel: PC amplitudes of the first 3 EOFs for the 7 biggest rapid ice change events corresponding to the top 23 % events. Bottom panel: PC amplitudes of the first 3 EOFs for the remaining 23 rapid ice change events. For the lowermost two panels, vertical offsets are used for visual clarity only.

OSD
9, 2327–2373, 2012

Arctic rapid sea ice loss events

R. Döscher and T. Koenigk

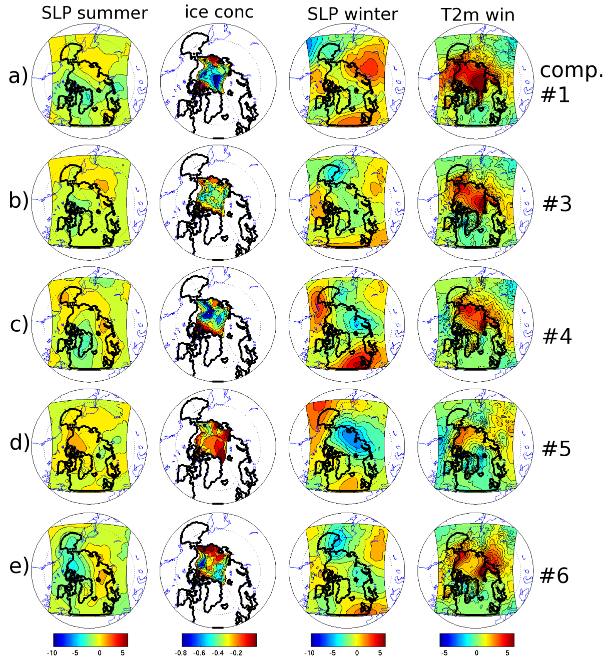

Fig. 6. Composite anomalies of summer SLP (hPa), september sea ice concentration, winter SLP (hPa) and winter T2m (K); based on the **(a)** warmest winter anomalies before a summer ice reduction event, **(b)** the lowest sea ice concentrations in the summers of the ice reduction event, **(c)** the strongest sea ice extent reductions, **(d)** the strongest cases of sea ice export during summer, **(e)** the weakest cases of sea ice export during summer. Anomalies are calculated as difference between the conditions during the event year and the average of 10 yr before the event.

OSD
9, 2327–2373, 2012

Arctic rapid sea ice loss events

R. Döscher and T. Koenigk

Title Page
Abstract Introduction
Conclusions References
Tables Figures
Back Close
Full Screen / Esc
Printer-friendly Version
Interactive Discussion

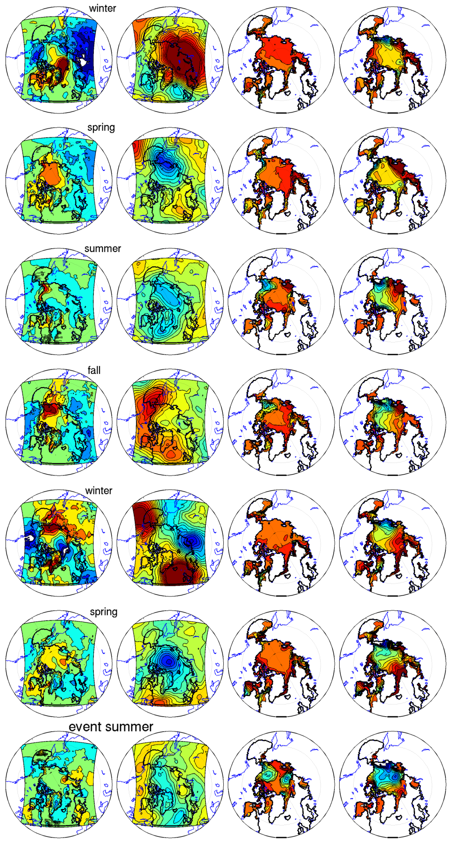

Fig. 7. CASE1: a sequence of seasonal means for case 1, with T2m (1st column, in K), SLP (2nd column, in hPa), SIC (3rd column) and ice thickness (4th column, in cm). Rows represent seasonal means starting in winter (JFM) 1997 and ending with the summer event 1998.

OSD
9, 2327–2373, 2012

R. Döscher and T. Koenigk

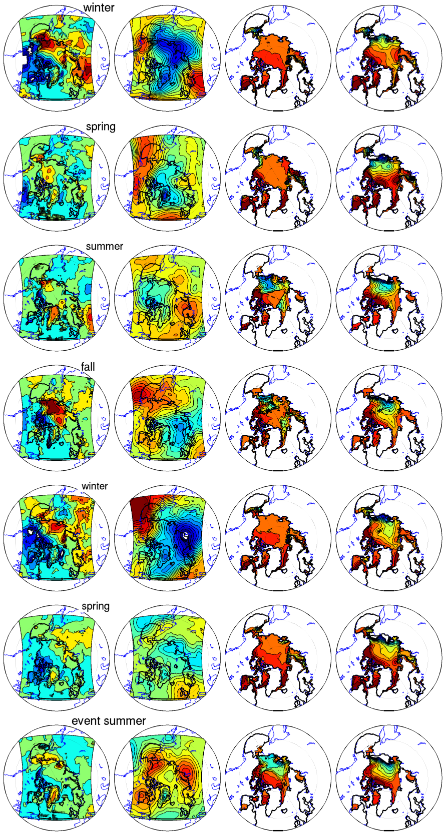

Fig. 8. CASE16: a sequence of seasonal means for case 16, with T2m (1st column, in K), SLP (2nd column, in hPa), SIC (3rd column) and ice thickness (4th column, in cm). Rows represent seasonal means starting in winter (JFM) 2032 and ending with the summer event 2033.

Discussion Paper | Discussion Paper | Discussion Paper | Discussion Paper |

OSD

9, 2327–2373, 2012

Arctic rapid sea ice loss events

R. Döscher and T. Koenigk

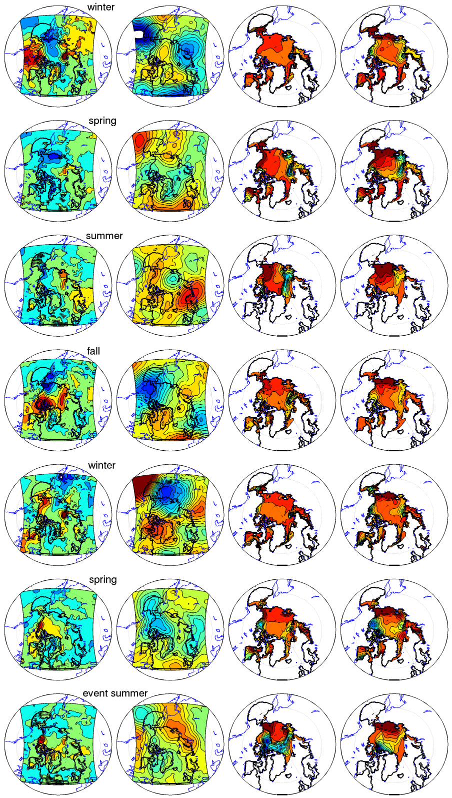

Fig. 9. CASE26: a sequence of seasonal means for case 26, with T2m (1st column, in K), SLP (2nd column, in hPa), SIC (3rd column) and ice thickness (4th column, in cm). Rows represent seasonal means starting in winter (JFM) 2024 and ending with the summer event 2025.

OSD
9, 2327–2373, 2012

R. Döscher and T. Koenigk

Title Page
Abstract | Introduction
Conclusions | References
Tables | Figures
◀I | ▶I
◀ | ▶
Back | Close
Full Screen / Esc
Printer-friendly Version
Interactive Discussion